Additive Manufacturing Letters 14 (2025) 100293

Contents lists available at ScienceDirect

Additive Manufacturing Letters

journal homepage: www.elsevier.com/locate/addlet

Short Communication

A practical guide to hydrogel working curves for bioprinting

Rion J. Wendland [a,*], Thomas J. Kolibaba [a], Kristan S. Worthington [b], Jason P. Killgore [a,*]

[a] Applied Chemicals and Materials Division, National Institute of Standards and Technology, Boulder, CO USA
[b] Roy J. Carver Department of Biomedical Engineering, University of Iowa, Iowa City, IA, USA

ARTICLE INFO

Keywords:
Hydrogels
Working curve
Jacobs equation
Photopolymerization
3D printing

ABSTRACT

The working curve is a widely implemented, but presently not standardized, method of assessing resin printability for photopolymer additive manufacturing technologies. While the working curve has been studied and refined for plastic resins, application to hydrogel materials used in bioprinting has been limited. Hydrogels present measurement challenges due to their decreased solids content, compliant nature, and significant swelling. Here, adapting lessons learned from interlaboratory studies on plastic working curves, we assess various techniques for hydrogel working curve measurements. Notably, across several formulations with various molecular weights and solids content, hydrogels exhibit near ideal log-linear behavior consistent with the Jacobs model when measured appropriately. However, certain measurement modalities (such as contact-based and rheological) can indicate Jacobs-like behavior, but with systematic errors in the cure depth compared to non-contact optical methods. Overall, this work highlights the challenges when conducting hydrogel working curve measurements and provides several considerations to help further develop and standardize measurements across 3D bioprinting applications.

1. Introduction

The use of photopolymer additive manufacturing (PAM) is widely established in the biomedical field, with applications including tissue engineered cell scaffolds, pharmaceutical delivery platforms, and microfluidic organ-on-a-chip devices [1–5]. Specifically, vat photopolymerization, which includes stereolithography and digital light processing systems, enables the creation of complex parts and structures in a fast and reproducible manner. Given the growth and impact of bioprinting on the healthcare system, it is imperative to develop measurement techniques to compare bioprinting materials accurately and reproducibly across laboratories and research groups.

In vat photopolymerization, an established measurement of photopolymer resin printability is the working curve. A common model used to understand the working curve is the Jacobs model. This model defines a relationship between Beer-Lambert light absorption and the critical exposure of light E_c necessary for liquid-to-solid polymerization [6]:

$$C_d = D_p \ln\left(\frac{E_0}{E_c}\right)$$

Here, C_d is the cure depth or thickness of a sample and E_0 is the incident radiant light exposure. When cure depth as a function of incident radiant exposure is determined experimentally, a log-linear plot produces slope D_p (light penetration depth: where light intensity attenuates to $1/e \approx 37$ %) and x-intercept E_c (Fig. 1). While historically E_0 is referred to as a "dose" rather than "radiant exposure", a "dose" is not consistent with the SI unit system. Here, we use "radiant exposure" or "exposure" to refer to the area-normalized optical energy input into the system [7]. Ideally, measuring a resin's working curve can enable users to determine suitable printing parameters (e.g., light intensity, cure time, layer thickness) for specific resins. Practically, these values can also be used as a quality control metric across resin batches, as well as an estimation of a resin's z-resolution and throughput capabilities.

In the field of plastic PAM (i.e. PAM wherein plastic or elastomeric materials are printed), the working curve has been the focus of many studies related to new measurement techniques [8–10], assumptions of the Jacobs equation [11–14], or characterizations of new photopolymer resins [15–18]. Despite the importance of the working curve, this measurement has yet to be standardized. For example, a recent interlaboratory study highlighted the variation of working curve measurements across laboratories, with up to a 7-fold and 70-fold difference in reported D_p and E_c values, respectively [19]. Importantly, some of this variation can be attributed to spectral variability of commercial printers, most notably broadband light sources and variable exposure across the

* Corresponding authors.
E-mail addresses: rion.wendland@nist.gov (R.J. Wendland), jason.killgore@nist.gov (J.P. Killgore).

https://doi.org/10.1016/j.addlet.2025.100293
Received 11 March 2025; Received in revised form 9 May 2025; Accepted 22 May 2025
Available online 22 May 2025
2772-3690/Published by Elsevier B.V. This is an open access article under the CC BY license (http://creativecommons.org/licenses/by/4.0/).

resin vat [20]. As such, the use of a well characterized and reproducible light source is vital for standardized working curve measurements. This is clearly demonstrated in the most recent interlaboratory study on plastic working curves, which made use of a standardized and well characterized LED light engine. This protocol resulted in significant improvements to the variations in D_p from 7-fold down to 1.6-fold and E_c from 70-fold down to 2.1-fold [21].

The rapid adoption of vat photopolymerization for bioprinting has accelerated the need for robust hydrogel characterization methods. Bioprinting typically uses hydrogel resins for their advantageous properties such as biodegradability, biocompatibility, and close approximation of natural tissue mechanics [22–24]. These hydrogel precursor materials can be synthetic (e.g., polyethylene glycol, polyacrylamide, polycaprolactone) or natural (e.g., gelatin, silk, hyaluronic acid) which each come with corresponding advantages and disadvantages [25,26]. The working curve measurement could provide a means of comparing resins properties and print-relevant parameters between different materials, batches, or laboratories. Additionally, the magnitude of D_p and E_c can provide important insights to bioprinting with live cells. For example, many live cell printing applications look to minimize the total energy exposure per layer to mitigate potentially harmful effects to the cells. Resins with low E_c would be prime candidates for live cell printing, as less energy exposure is needed to polymerize the layer. Likewise, high D_p resins would potentially minimize the overall radiant exposure to the cells but may negatively impact the achievable resolution of the printed structure. Regardless of material, implementing working curves on hydrogels requires rethinking of the cure depth (thickness) measurement due the low stiffness samples (kPa to MPa) that could be easily deformed or damaged by typical contact-based thickness measurement tools like handheld micrometers [27–29]. As an alternative, some groups have used non-contact methods such as microscopy or photorheology to measure working curve behavior on a variety of photopolymer materials [10,19,30,31]. However, there remains a gap in understanding and quantifying how different measurement methods influence hydrogel working curves and Jacobs parameters.

Here, we present a guide to practical considerations for measuring working curves on hydrogel systems. We use a model acrylate polymer, polyethylene glycol diacrylate (PEGDA), at various molecular weights and concentrations to compare how different cure depth measurement techniques influence hydrogel working curve fit parameters. For all measurement techniques, we use an identical light source to ensure that true comparisons can be made between methods. Importantly, we show that working curve measurements of photopolymer hydrogels cured with a well-calibrated, narrowband LED light source produce the log-linear working curve relationship predicted from the Jacobs model. However, working curves and the extracted E_c and D_p parameters are strongly dependent on the measurement method. Contact methods substantially compress soft samples, resulting in an underestimation of cure depth which effects the D_p and E_c values extracted from the Jacobs model fits. On the other hand, optical methods do not substantially deform samples but require appropriate contrast and analysis techniques to accurately determine cure depth. Gap-dependent photorheology is also investigated as a candidate measurement technique, but the resultant cure profiles do not predictably correlate to either the contact or optical methods. Overall, the results presented here can be applied to all hydrogel photopolymer 3D printing applications, helping to further develop and standardize working curve measurements across the field.

2. Materials and methods

Certain commercial equipment, instruments, or materials are identified in this paper to specify the experimental procedure adequately. Such identification is not intended to imply recommendation or endorsement by NIST.

2.1. Materials

Polyethylene glycol diacrylate (PEGDA, $M_w = 700$ Da and $M_w = 575$ Da) and tartrazine were purchased from Sigma Aldrich (St. Louis, MO, USA). PEGDA ($M_w = 3400$ Da) was purchased from Thermofisher Scientific (Waltham, MA, USA). The photoinitiator lithium phenyl-2,4,6-trimethylbenzoylphosphinate (LAP) was purchased from Colorado Photopolymer Solutions a subsidiary of Arkema (King of Prussia, PA, USA). All chemicals were used as received.

2.2. Hydrogel formulations

Three water-based hydrogel formulations were used for experimentation. A “stiff” hydrogel consisted of 40 % by mass PEGDA 700 in deionized water, while two “soft” hydrogels consisted of 10 % by mass PEGDA 700 or 20 % by mass PEGDA 3400 in deionized water. These formulations were chosen as a generalized subset of hydrogels, including differences in both molecular weight and PEGDA concentrations. For comparing working curve parameters, three additional hydrogel formulations were used: 20 % by mass PEGDA 700, 10 % by mass PEGDA 575, and 25 % by mass PEGDA 575, all in deionized water. All formulations contained photoinitiator LAP at 1 % by mass and photoabsorber tartrazine at 0.1 % by mass. Formulations were stored protected from light prior to use. All measurements were performed with samples polymerized from the same batch of a given resin, and resins were refrigerated (4 °C) and kept in the dark when not in use.

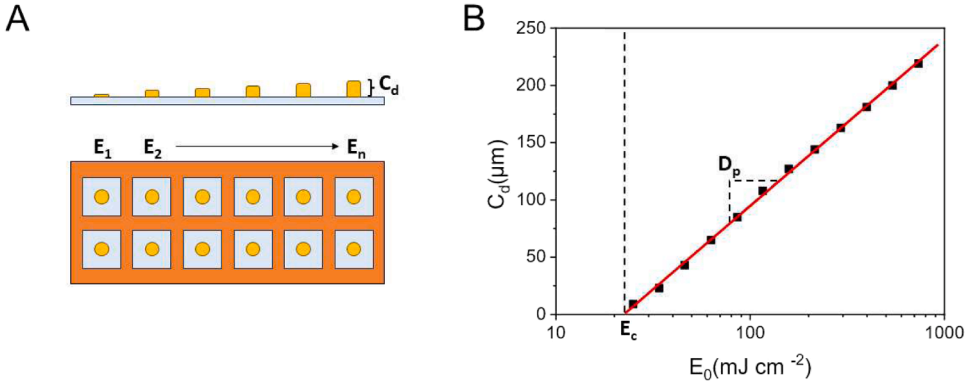

Fig. 1. Example schematic of a working curve experiment. **A**) Photopolymer formulations are irradiated for discrete exposure durations in isolated areas of a methacrylate-functionalized glass slide and the resulting cure depths are measured. **B**) Cure depths are plotted against radiant exposure on a log-linear plot: D_p is the slope of the regression while E_c is the x-intercept.

2.3. Light source

To photopolymerize the hydrogel samples for working curve measurements, a collimated LED (Solis-405C LED, Thorlabs; Newton, NJ) light source with a 2.5 mm aperture was used. Light was filtered using a 1.9 nm bandpass filter centered at 405 nm (**Figure S1**). The LED drive current was 370 mA, which resulted in an irradiance of 8.0 mW cm^{-2}, as measured using an integrating sphere photodiode power meter (S142C, Thorlabs).

2.4. Hydrogel fabrication

For working curve generation (except photorheology), hydrogel resins were polymerized onto glass slides functionalized with 3-(trimethoxysilyl) propyl methacrylate (Automate Scientific; Berkeley, CA, USA), using 1.6 mm thick silicone isolators (Grace Biolabs; Bend, OR) to ensure sufficient resin volume greater than any achieved cure depth (max cure depth was <400 μm in this study). After curing, samples were measured for cure depth within one hour using a variety of techniques.

2.5. Cure depth measurements

To measure the cure depth of hydrogel samples and generate a working curve, six different analytical techniques were used:

2.5.1. Handheld micrometer (HHM)

A flat anvil thickness gauge (Mitutoyo 547-500S; Aurora, IL) is a commonly used device in plastic working curve measurements. Here, the micrometer was used to measure sample thickness immediately after polymerization. Due to the design of the micrometer head, the silicone isolator was removed from the glass slide, and samples briefly rinsed with water prior to measuring. It should be noted that this is the only technique that did not measure hydrogel cure depth while immersed in resin.

2.5.2. Low force micrometer (LFM)

A low force micrometer (Mitutoyo Litematic VL-50A) with a 3 mm diameter sphere head and contact force of 0.01 N was used to measure cure depths immediately following polymerization while samples were still immersed in the hydrogel resin.

2.5.3. Nanoindenter (NI)

A nanoindentor (Bruker, Hysitron TI 950 TriboIndenter; Billerica, MA) equipped with a 100 μm radius conospherical probe and contact force of 20 μN was used to measure cure depths while samples were still immersed in the hydrogel resin. As the probe approached each hydrogel sample, the X, Y, and Z coordinate positioning of the contact were recorded. To ensure accurate measurements of sample heights, the probe was also lowered onto three corners of the glass slide. These coordinates were recorded and fit to an equation describing the reference plane. Sample heights were then calculated using their recorded coordinates and positioning relative to the reference plane.

2.5.4. Photorheometer (PR)

A rheometer (Netzsch, Kinexus Ultra+; Selb, Germany) equipped with a glass bottom plate and an 8 mm parallel plate upper geometry was used to assess the suitability of using photorheology to generate a working curve. The Solis 405 filtered light source was placed underneath the rheometer and calibrated using the power meter to an irradiance of 8.0 mW cm^{-2}. For all samples, a single-frequency strain controlled oscillatory sequence at a frequency of 1 Hz and strain amplitude of 0.1 % was executed at increasing gap heights from 50 μm to 350 μm. Here, contrary to traditional working curve measurements, samples are continuously irradiated while measuring a rheological time-domain signal under a fixed gap height. From the rheological data, the time at which the polymerized gel spanned the gap is determined and used to calculate a radiant exposure [30,31]. By measuring samples across several gap heights, a working curve-like relationship can be plotted. We tried several methods for determining exposure time to reach full gap height, yet none provided unambiguous agreement with other working curve measurement methods (**Figure S2**). Herein, we show the method of using the time after irradiation elapsed before the shear storage modulus significantly increased above the baseline (G' Delay, time at which slope of shear modulus data greater than 2 Pa/s) [30,31].

2.5.5. Optical coherence tomography (OCT) apparatus

OCT is a non-invasive imaging technique which uses near-infrared light to detect contrast from differences in light scattering throughout a sample. Here, an OCT (Thorlabs Ganymede, 880 nm, GAN632C1) system was used to obtain images of hydrogel samples and extract cure depths while samples were still immersed in the hydrogel resin. OCT images were collected at 10 kHz with 5 A-scan averages and 4 B-scans per slice.

To measure sample cure depth, the average height across the center of the sample was calculated based on number of pixels from glass slide to the top of the sample and the refractive index of each resin (**Figure S3C**). As the z-scale of OCT images is dependent of the refractive index of the sample, the refractive index of each hydrogel resin and polymerized sample was calculated using a reference height imaged through air (refractive index of 1.00). To verify calculations, the reference height was also recorded as imaged in water, which confirmed a refractive index of 1.33 (**Figure S3A**).

PEGDA 3400 samples had increased water content compared to PEGDA 700 samples and were not able to be resolved from the surrounding ink. To identify the sample boundary, tungsten beads (nominal diameter of 12 μm, Sigma Aldrich) were used. The tungsten beads were first added at 50 mg mL^{-1} in water, mixed vigorously, and one drop was added to each sample well after polymerization. To confirm addition of the beads did not influence the measured cure depth, a working curve of 10 % PEGDA 700 was constructed with and without beads, which resulted in no significant differences between techniques (**Figure S3B, D**).

2.5.6. Laser scanning confocal microscopy (LSCM)

A laser scanning confocal microscope (Nikon AXR) was used to measure cure depth of hydrogel samples. Following polymerization, resin was removed from the isolator wells and fresh resin containing 0.2 % by mass red fluorescent labeled polystyrene microbeads of 1 μm diameter (580/605 FluoSpheres, ThermoFisher Scientific) added to the wells. Z-stack images with 2 μm pitch were obtained (561 nm excitation laser and 575 nm – 625 nm emission filter) for each sample and analyzed using ImageJ to find the glass slide interface and heights of the samples using the signal from the fluorescent beads (**Figure S4**).

Additionally, the ability of confocal microscopy to directly measure cure depth was tested. To obtain fluorescently labeled samples, 0.1 % by mass of fluorescein isothiocyanate (FITC)-conjugated PEG acrylate (MW 2000, PEGWorks, Chapel Hill, NC) was included in the resin formulations. FITC-PEG was dissolved at 100 mg mL^{-1} and added to the 10 % PEGDA 700 formulation at a final concentration of 0.1 % by mass. This low concentration of a non-crosslinking species is not expected to significantly impact the curing kinetics nor working curve calculations. FITC-PEG samples were imaged using 488 nm excitation laser and 500 nm – 550 nm emission filter.

Specific metrics of each measurement technique can be found below (Table 1).

2.6. Hydrogel modulus measurements

To determine hydrogel modulus for each formulation, samples were fabricated with the same light source described above, using a mold consisting of a functionalized glass slide, 50 μm PTFE shim stock spacers

Table 1
General properties of analytical techniques used to measure cure depth of hydrogels. Uncertainty of OCT height resolution is a result of differences in the refractive index of hydrogel resins.

	Method	Measuring force/ mechanism	Height resolution	Contact point
HHM	Contact	≤ 1.5 N	10 μm	Ø 10 mm anvil
LFM	Contact	0.01 N	1 μm	Ø 3 mm sphere
NI	Contact	20 μN	0.1 μm	Ø 0.2 mm sphere
PR	Real time	0.1 % Shear Strain	0.1 μm	Ø 8 mm plate
OCT	Non-contact	Refractive Index	~1.2 μm	-
LSCM	Non-contact	Fluorescence	1 μm	-

(McMaster-Carr), and a non-functionalized glass slide, held together using binder clips. For each formulation, "overcured" samples were irradiated for an exposure that would create a 300 μm sample in an unconstrained environment, as determined by the optical working curve measurements (40 % PEGDA 700: 14 s, 10 % PEGDA 700: 35 s, 20 % PEGDA 3400: 60 s). These exposures were chosen to minimize the gradient of crosslinking density through the sample thickness. Nanoindentation (Bruker, Hysitron TI 950 TriboIndenter) was performed using a 20 μm radius conospherical probe, while samples were immersed in water. Notably, the automated surface detection method on the nanoindentor has a minimum detection force of approximately 2 μN. At this force, there is insufficient displacement range to fully withdraw from all the samples. As a workaround, after using the built-in sequence to find the sample surface, a displacement control method was performed where the probe would retract 2 μm before traveling a total of 4 μm in the direction of the sample. This approach ensured that a zero-force baseline was observed prior to engaging with the sample. Four load-displacement curves for each formulation were collected and fit to the Hertz contact model to calculate reduced modulus values.

2.7. Statistical analysis

For each hydrogel formulation, a one-way ANOVA with Tukey's post-hoc test was conducted (95 % confidence interval) to compare the calculated D_p and E_c values from each measurement technique. Working curve samples were fabricated and measured in triplicate from a single batch of hydrogel resin to better understand the variability of the measurement techniques. Origin Pro, Version 2024 was used for all statistical analyses and generating plots.

3. Results and discussion

To provide a practical guide to hydrogel working curves, we used several techniques to measure the cure depth versus radiant exposure of various hydrogel formulations. Regardless of measurement method or hydrogel formulation, near-ideal log-linear, Jacobs-like behavior was observed (Fig. 2). In plastic working curves, improved log-linear behavior can be obtained using a 2 nm bandpass-filtered LED light source compared to unfiltered LED light which is directly correlated to reducing the inner-filter effect in the resin [12]. Here, the filtered light source appeared to be similarly effective at achieving log-linear behavior despite additional complications from swelling and chemical mobility in hydrogels. However, despite the general log-linear behavior, the actual working curves varied considerably depending on measurement method. The 40 % PEGDA 700 resin served as a stiff control sample (reduced modulus: 8500 kPa) and demonstrated consistent curves for all techniques except photorheology (Fig. 2A). On the other hand, for low stiffness resins (10 % PEGDA 700, reduced modulus: 31 kPa and 20 % PEGDA 3400, reduced modulus: 160 kPa) contact methods (HHM, LFM, and NI) caused deformation of the hydrogel samples which resulted in lower cure depth measurements when compared to optical techniques

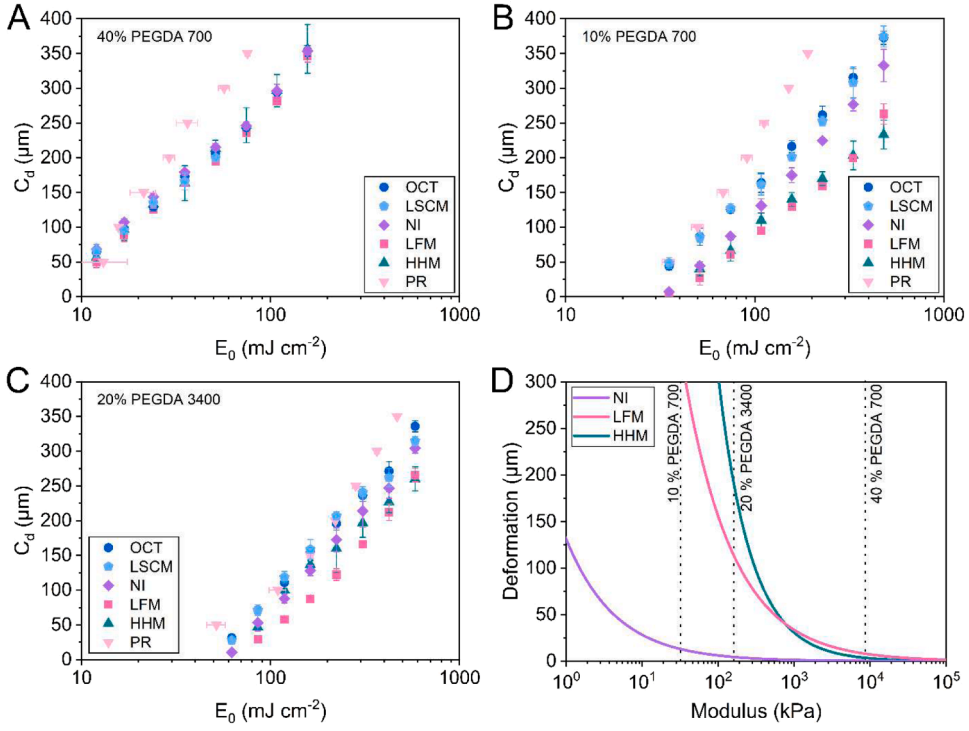

Fig. 2. Cure depth vs exposure data using each measurement technique for **A**) 40 % PEGDA 700, **B**) 10 % PEGDA 700, and **C**) 20 % PEGDA 3400 hydrogels. $n = 3$; data represent mean ± standard deviation. **D**) Estimated deformation of a sample with a given modulus using contact methods of measuring cure depth. Deformation is calculated using Hertz (NI, LFM) and cylindrical (HHM) contact mechanics and the associated parameters of the measurement systems. Dotted lines indicate magnitude of hydrogel reduced modulus as measured using nanoindentation.

(OCT and LSCM) (Fig. 2B-C). These observations can be explained from elastic compression for HHM or Hertzian contact mechanics for LFM and NI. In each case, measured hydrogel modulus values and instrument parameters can begin to account for discrepancies between techniques (Fig. 2D, Table 1). These relationships clearly demonstrate how contact methods can result in inaccuracies when measuring cure depths, especially for hydrogel samples. The estimated deformations become significant (i.e., of similar order to cure depth or layer thickness) in the reported range of hydrogel moduli (10 s to 100 s of kPa). Importantly, the contact-based methods will minimize deformation when force is reduced, and indenter or platen size is increased. For example, using atomic force microscopy protocols [32], deformations <1 μm could be achieved on hydrogels with 1 kPa modulus when measured at 3 nN force with a 10 μm radius indenter. However, most atomic force microscopes lack sufficient travel distance in the Z-direction piezo to probe print-relevant cure depths (tens to hundreds of micrometers), requiring customization or a workaround utilizing coarse positioning motors. While these models provide a framework for estimating sample deformation, it is important to note the underlying assumption that the modulus is constant throughout the sample. Numerous studies have demonstrated a conversion and modulus gradient in the z-direction of photopolymerized samples (e.g. 10-fold modulus gradient through a typical layer) [33], particularly in 3D printed parts [34–37]. These gradients and other physical phenomena such as sample dimensional changes under load likely account for the differences between the predicted and observed (treating OCT as ground truth) deformations (**Table S1**). Though there are no simple analytical solutions to modulus gradients in the context of contact mechanics, developing models of how mechanical property gradients are imparted on hydrogel structures would be impactful, given the sensitivity of cell behavior to the surrounding environment [38–40].

As noted above, the photorheology data departed from the optical and mechanical measured data. From the photorheology data, a clear trend was observed that increasing the gap height results in a longer delay time to increase the shear modulus of the sample above baseline (**Figure S2**). However, none of the methods for determining the time at which a sample reached the constant gap heights resulted in working curves that were closely matched across all gap heights to the other cure depth measurements (Fig. 2A-C). Interestingly, for 20 % PEGDA 3400 samples, photorheology data at small gap heights (< 250 μm) were more closely matched to optical techniques before deviating at large gap heights (Fig. 2C). Here, it is important to note the differences between photorheology and other techniques. Though aperture size between the traditional working curve measurements and photorheology were different, working curve measurements are relatively insensitive to aperture size at these length scales (**Figure S5**). Additionally, the rheometer setup results in a fixed boundary condition between the parallel plates which may impact reaction kinetics, and there is potential for back-reflection off the top plate, increasing the effective irradiance. However, a more significant consideration is how real time rheology measurements are influenced by large, dynamic mechanical property gradients in the sample. For example, with larger gap heights, the rheometer may be sensitive to changes throughout the thickness of the sample and register an increase in mechanical properties before the cure front truly reaches the full gap. This would lead to underestimations of the required radiant exposure for each gap height, which is observed in these experiments. For the 20 % PEGDA 3400 samples, the high E_c and low stiffness of this formulation could act in combination to counteract the 'underestimations' at small gap heights, while large gap heights are still subject to the signal issue of evolving mechanical property gradients. Given the large differences in apparent C_d between photorheology and direct cure depth methods, understanding the evolving mechanical property gradients across the gap height is central to properly interpreting these measurements. Though many studies have related photopolymer modulus evolution with spectroscopically measured conversion [41–43], spatially resolved comparisons of modulus gradients and cure depth would likely be needed to validate future relationships and models.

While optical (OCT, LSCM) methods do not result in sample deformations, they do present separate challenges for hydrogel samples. Namely, these measurement techniques require significant optical contrast between the sample and background, which can be difficult to achieve for hydrogel samples primarily composed of water. For OCT imaging, the two resins consisting of PEGDA 700 were able to be directly measured. However, for the 20 % PEGDA 3400 hydrogels, samples were unable to be resolved from the surrounding resin and the addition of tungsten beads was required to outline the sample (**Figure S3**). This is likely due to the increase of water content per crosslinked chain, which is related to the swelling ratio of the hydrogel, shown to increase with increasing molecular weight of PEGDA [44,45]. For LSCM, fluorescent beads were added to the sample wells after polymerization to obtain sample outlines and measure cure depth. However, this bottom-up imaging approach fails if fluorescent signals are unable to be detected through a sample, either from light scattering or absorption (e.g., 40 % PEGDA 700 samples at longer exposures). If a sample were naturally fluorescent, the addition of particles or dyes would not be required, as demonstrated by the addition of a FITC-labeled PEG monomer to the hydrogel resin (**Figure S4**). However, there may remain uncertainties to where the edge of the cure front is located when imaging submerged hydrogels without distinctive boundaries. Importantly, both OCT and LSCM were in close agreement for cure depths across all formulations, adding confidence that optical techniques with micron-scale z-resolution are among the most accurate methods for hydrogel cure depth measurements.

From the working curve plots, cure depths of a photopolymer resin can be related to radiant exposures using the Jacobs equation. The log-linear regression gives two fit parameters: D_p (light penetration depth, the slope) and E_c (critical exposure, the x-intercept) (Fig. 3, **Table S2**). It should be noted that the light penetration depth of a resin can be directly measured using UV–Vis spectroscopy (herein referred to as "optical D_p"). The Jacobs model D_p ("working curve D_p") is a fit parameter which is not directly adapted from the optical D_p, but instead encodes kinetics and gelation into the calculation. Despite these differences, the optical D_p and working curve D_p of a polymer system generally follow similar trends. In this study, initiator and dye concentrations were consistent across the three hydrogel resins, and thus a similar optical D_p was expected and observed when measured using UV–Vis absorbance data (**Figure S6**). While a slight decrease in optical D_p for 40 % PEGDA 700 resin was observed, this may be due to the large increase in PEGDA concentration and solids content increasing the density of the solution, which increases the molar concentration of the absorbing species. Notably, it is implicit in the Jacobs model that both the resin and polymerized sample have equivalent absorbance that do not change as a function of time or cure. Effects such as polymer shrinkage and swelling are thus not accounted for in the Jacobs model. In all hydrogel formulations, the working curve D_p fit parameters were consistently higher than the spectroscopic D_p, especially for optical (OCT, LSCM) methods (Fig. 3A, C, E). A working curve D_p higher than the optical D_p is consistent with polymer swelling commonly observed in hydrogel systems (as opposed to shrinkage of plastic resins). Interestingly, the soft hydrogel formulations (10 % PEGDA 700 and 20 % PEGDA 3400), which would be anticipated to have more significant swelling, had larger increases in the working curve D_p vs. the optical D_p than the stiff 40 % PEGDA samples (**Table S2**). These discrepancies have been observed in the literature [46], and can be attributed to physical deviations for the Jacobs equation assumptions. Consideration of both the optical and working curve D_p values may be important in bioprinting. The optical D_p could indicate the depth extent of reaction that results in the necessary interlayer adhesion for printing. The working curve D_p on the other hand should correspond to geometric variations in the final printed structures. Compared to optical measurements, contact methods on the soft hydrogels had increased deformation of taller samples, resulting in

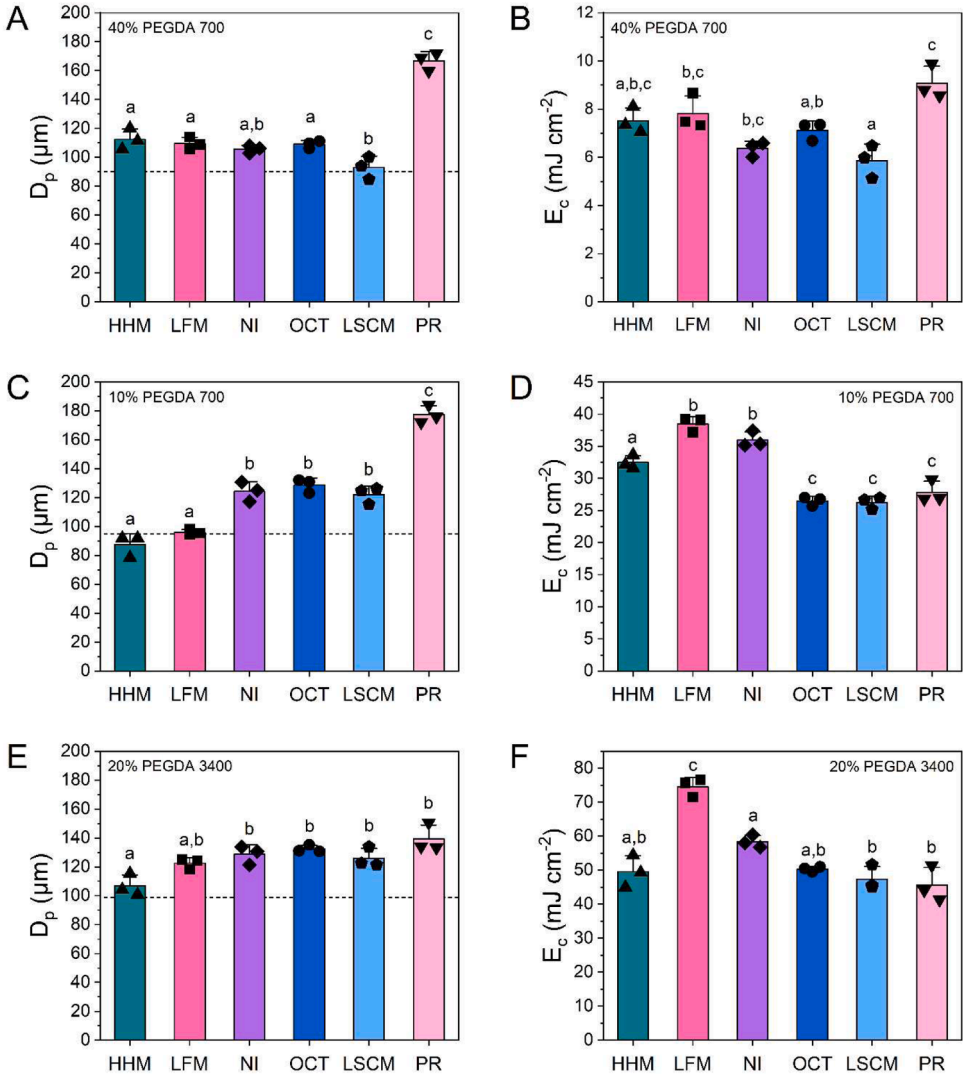

Fig. 3. D_p and E_c parameters calculated from a log-linear regression for **A,B**) 40 % PEGDA 700, **C,D**) 10 % PEGDA 700, and **E,F**) 20 % PEGDA 3400 hydrogels for each measurement technique. $n = 3$; data represent mean ± standard deviation. Dashed lines in **A,C**, and **E** represent the D_p measured using UV–Vis spectroscopy. Means that do not share a letter are significantly different ($p \leq 0.05$).

decreased working curve D_p values. Of note, HHM working curve D_p values were significantly different from optical methods for both soft hydrogels while NI working curve D_p were not statistically different ($p \leq 0.05$, Fig. 3, **Table S3–5**). Relative errors (compared to optical methods) of working curve D_p for these soft hydrogels ranged from <1 % (NI) to greater than 30 % (HHM). If the deformation was constant across all samples, the working curve D_p would be expected to be consistent. This nonuniform deformation is likely a result of modulus gradients throughout photopolymerized samples, further highlighting the challenges of these measurements. Photorheology working curves typically overestimated working curve D_p compared to all other methods. Again, it is important to note that photorheology is not directly measuring a cure depth but is instead a more nuanced real-time measurement.

The other Jacobs equation parameter (E_c) is closely related to the monomer and crosslinker species of the resin, and is sensitive to differences in concentration, molecular weight, reactivity, and crosslinking density. Based on photopolymerization fundamental equations, in general, higher local concentrations of reactive groups and higher reactivity ratios are expected to yield lower E_c values. This is clearly demonstrated in the three different hydrogel resins, as the 40 % PEGDA 700 had the lowest E_c followed by 10 % PEGDA 700 and 20 % PEGDA 3400 (Fig. 3B, D, F). Interestingly, for the LSCM of 40 % PEGDA 700, a slight decrease was seen in both D_p and E_c. This is likely due to the fact that longer exposure samples were unable to be measured, which had a significant influence on the fitting of the logarithmic Jacobs equation. When comparing across measurement techniques, contact methods (HHM, LFM, NI) generally had higher E_c values than optical methods (OCT, LSCM) for soft hydrogels, due to the deformation of samples during measurement. For 10 % PEGDA 700, E_c from all contact method methods were significantly different from optical E_c, while only LFM E_c was statistically different from optical methods for 20 % PEGDA 3400 ($p \leq 0.05$, Fig. 3, **Table S3–5**). Relative errors (compared to optical methods) of E_c for soft hydrogel samples ranged from 1 % to 50 %. Importantly, regardless of measurement technique used, the rank order of E_c (40 % PEGDA 700 < 10 % PEGDA 700 < 20 % PEGDA 3400) is maintained, suggesting each technique could be used as a general comparison tool.

Treating the OCT data as ground truth, insights into hydrogel printability can be observed in the calculated working curve parameters. For example, measuring the working curve of three additional PEGDA formulations (20 % PEGDA 700, 10 % PEGDA 575, and 25 % PEGDA 575), E_c can be compared to the concentration of reactive functional groups (acrylates) in each resin (Fig. 4, **Table S6**). While decreasing E_c values as functional group concentration increases are expected based

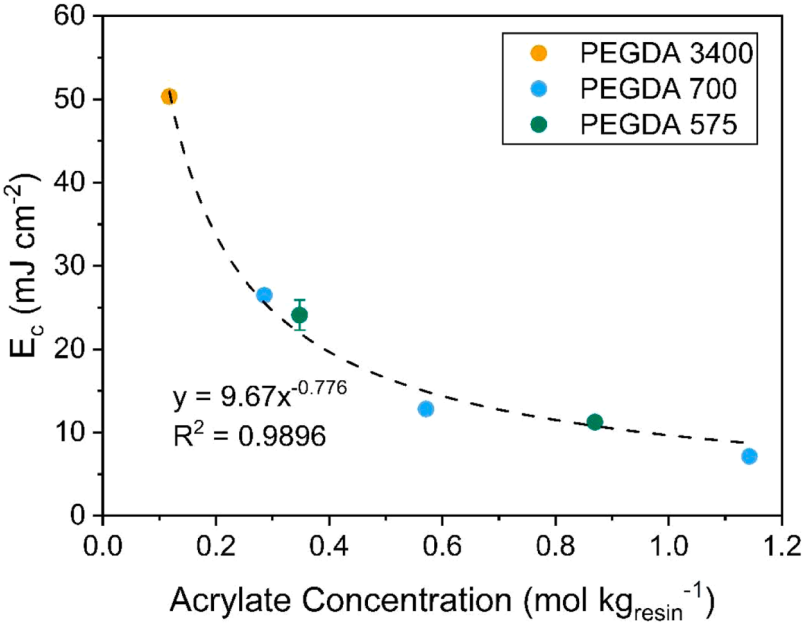

Fig. 4. OCT-calculated E_c versus acrylate functional group concentration for several hydrogel formulations with a power law best fit equation. $n = 3$; data represent mean ± standard deviation.

on photopolymer reaction kinetics, it is significant that a simple fit equation with low residuals can describe this relationship across multiple PEGDA molecular weights and concentrations. It should be noted that all formulations in this study contained consistent photoinitiator and dye concentrations, and thus future studies should continue expand the scope of these observations. Interestingly, coupling this observation with a spectroscopic (e.g., infrared spectroscopy) or spectro-photo-mechanical (e.g., photorheology coupled with Raman spectroscopy) technique would extract conversion information from these systems. This information could be used to develop a chain-growth analog to the Carothers equation [47] and grant significant predictive power in bioink design and potentially even in plastic printing.

Overall, the results presented here help to lay the groundwork for measuring and standardizing the working curve measurement of hydrogel systems. While contact methods (specifically handheld micrometers and low force micrometers) of measuring cure depth may be simple and cost effective, the inaccuracies of cure depth measurements due to sample deformation limit their use. On the other hand, optical techniques result in more accurate measurements of hydrogel cure depths, but can be limited by cost, availability, and sample processing. For example, in confocal imaging, the addition of fluorescent dyes or particles was required to image the hydrogel samples. Regardless, as many hydrogel systems (beyond PEG-based) have similar mechanical and optical properties, these results are applicable to a broad range of materials, including natural polymers derived from gelatin, chitosan, or hyaluronic acid. Additionally, accurate measurement of hydrogel working curves can enable further quality control for bioprinting specific constraints. For example, for a given resin, changes in the initiator concentration will primarily influence E_c, with minimal changes to D_p while changes in dye concentration will primarily influence D_p and not E_c [46,48,49]. Given that increased initiator concentrations can drastically decrease cell viability [50,51], the working curve measurement can help to screen bioprinting resins for batch-to-batch processing variability. Overall, this work should be easily translatable across the bioprinting field, enabling the development, screening, and comparison of bioprinting resins.

4. Conclusion

For photopolymer additive manufacturing, the working curve has become ubiquitous in resin development and specification. However, a lack of standardization in the field has limited the practicality and applicability of this measurement. Additionally, much work in the field is based in plastic materials, which have drastically different properties compared to the hydrogel materials typically used in bioprinting applications. Given the importance of 3D printing in the healthcare field, it is imperative to better understand and develop measurements for hydrogel 3D printing. Here, we screened multiple common methods of measuring hydrogel cure depth and describe important considerations and comparisons of each technique. Overall, working curves for hydrogels are recommended to be measured using optical, as opposed to contact methods, to ensure sample deformation does not impact Jacobs model fitting parameters. Additionally, while real-time measurements such as photorheology offer an interesting insight into photopolymer reactions, more theoretical understanding of polymer cure profiles and mechanical property gradients are necessary for these techniques to be used for working curves. Generally, these results could be the foundation of bioprinting quality control systems, while also serving as a starting point for optimizing print parameters. This practical guide of hydrogel working curves will help to further advance not only bioprinting innovations, but all photopolymer additive manufacturing cases that use hydrogel systems.

CRediT authorship contribution statement

Rion J. Wendland: Writing – review & editing, Writing – original draft, Methodology, Investigation, Formal analysis, Data curation, Conceptualization. **Thomas J. Kolibaba:** Writing – review & editing, Methodology, Conceptualization. **Kristan S. Worthington:** Writing – review & editing, Resources. **Jason P. Killgore:** Writing – review & editing, Supervision, Project administration, Methodology, Funding acquisition, Conceptualization.

Declaration of competing interest

The authors declare that they have no known competing financial

interests or personal relationships that could have appeared to influence the work reported in this paper.

Acknowledgements

This research did not receive any specific grant from funding agencies in the public, commercial, or not-for-profit sectors.

This work was performed while Rion Wendland held a National Research Council Associateship Award at the National Institute of Standards and Technology. Photorheology was performed in the Worthington Lab at the University of Iowa. Fluorescent beads were obtained from the Burdick Biomaterials and Biofabrication Lab at the University of Colorado Boulder. The confocal laser scanning microscopy was performed at the University of Colorado Boulder BioFrontiers Institute Advanced Light Microscopy Core (RRID: SCR_018302). The Nikon AXR Laser Scanning Confocal is supported by NIH (National Institute of Health) grant 1S10OD034320.

Supplementary materials

Supplementary material associated with this article can be found, in the online version, at doi:10.1016/j.addlet.2025.100293.

Data availability

Data will be made available on request.

References

[1] S.T. You, et al., High cell density and high-resolution 3D bioprinting for fabricating vascularized tissues, Sci Adv. (8) (2023) 9, https://doi.org/10.1126/sciadv.ade7923.
[2] W. Kim, et al., 3D Inkjet-bioprinted lung-on-a-chip, ACS Biomater. Sci. Eng. 9 (5) (2023) 2806–2815, https://doi.org/10.1021/acsbiomaterials.3c00089.
[3] B.N. Allen, et al., Photopolymerization parameters influence mechanical, microstructural, and cell loading properties of rapidly fabricated cell scaffolds, ACS Biomater. Sci. Eng. 9 (5) (2023) 2663–2671, https://doi.org/10.1021/acsbiomaterials.3c00408.
[4] D.N. Kang, et al., 3D bioprinting of a gelatin-alginate hydrogel for tissue-engineered hair follicle regeneration, Acta Biomater. 165 (2023) 19–30, https://doi.org/10.1016/j.actbio.2022.03.011.
[5] A. Fritschen, et al., High-scale 3D-bioprinting platform for the automated production of vascularized organs-on-a-chip, Adv. Heal. Mater. (17) (2024) 13, https://doi.org/10.1002/adhm.202304028.
[6] P.F. Jacobs, Fundamentals of stereolithography, in: Proceedings of Solid Free Form Symposium, 1992, pp. 196–211.
[7] A. Thompson, B.N.T., guide for the use of the International system of units (SI), Natl. Inst. Stand. Technol. Spec. Publ. 811 (2008).
[8] C.I. Higgins, T.E. Brown, J.P. Killgore, Digital light processing in a hybrid atomic force microscope: in Situ, nanoscale characterization of the printing process, Addit. Manuf. (2021) 38, https://doi.org/10.1016/j.addma.2020.101744.
[9] J.P. Killgore, et al., A data-driven approach to complex voxel predictions in grayscale digital light processing additive manufacturing using U-nets and generative adversarial networks, Small (50) (2023) 19, https://doi.org/10.1002/smll.202301987.
[10] Y. Li, et al., Theoretical prediction and experimental validation of the digital light processing (DLP) working curve for photocurable materials, Addit. Manuf. (2021) 37, https://doi.org/10.1016/j.addma.2020.101716.
[11] L.M. Stevens, et al., Counting all photons: efficient optimization of visible light 3D printing, Adv. Mater. Technol. 8 (23) (2023), https://doi.org/10.1002/admt.202300052.
[12] B.W. Caplins, et al., Influence of spectral bandwidth on the working curve in vat photopolymerization, Addit. Manuf. (2024) 85, https://doi.org/10.1016/j.addma.2024.104172.
[13] H. Gong, et al., Custom 3D printer and resin for 18 μm x 20 μm microfluidic flow channels, Lab. Chip 17 (17) (2017) 2899–2909, https://doi.org/10.1039/c7lc00644f.
[14] P. van der Linden, A.M. Popov, D. Pontoni, Accurate and rapid 3D printing of microfluidic devices using wavelength selection on a DLP printer, Lab. Chip 20 (22) (2020) 4128–4140, https://doi.org/10.1039/d0lc00767f.
[15] T. Schlotthauer, D. Nolan, P. Middendorf, Influence of short carbon and glass fibers on the curing behavior and accuracy of photopolymers used in stereolithography, Addit. Manuf. (2021) 42, https://doi.org/10.1016/j.addma.2021.102005.
[16] J. Guit, et al., Photopolymer resins with biobased methacrylates based on soybean oil for stereolithography, ACS Appl. Polym. Mater. 2 (2) (2020) 949–957, https://doi.org/10.1021/acsapm.9b01143.
[17] S. Krishnamoorthy, et al., Investigation of gelatin methacrylate working curves in dynamic optical projection stereolithography of vascular-like constructs, Eur. Polym. J. (2020) 124, https://doi.org/10.1016/j.eurpolymj.2020.109487.
[18] C.W. Weyhrich, et al., Temporally stable supramolecular polymeric salts enabling high-performance 3D all-aromatic polyimide lattices, Small (32) (2023) 19, https://doi.org/10.1002/smll.202303188.
[19] T.J. Kolibaba, et al., Results of an interlaboratory study on the working curve in vat photopolymerization, Addit. Manuf. (2024) 84, https://doi.org/10.1016/j.addma.2024.104082.
[20] B.W. Caplins, et al., Characterizing light engine uniformity and its influence on liquid crystal display based vat photopolymerization printing, Addit. Manuf. (2023) 62, https://doi.org/10.1016/j.addma.2022.103381.
[21] Kolibaba, T., et al., Results of an interlaboratory study on the working curve in vat photopolymerization II: towards a standardized method. 2025. DOI: https://doi.org/10.2139/ssrn.5214256.
[22] W.D. Jia, et al., A multicrosslinked network composite hydrogel scaffold based on DLP photocuring printing for nasal cartilage repair, Biotechnol. Bioeng. 121 (9) (2024) 2752–2766, https://doi.org/10.1002/bit.28769.
[23] M. Zanon, et al., Visible light-induced crosslinking of unmodified gelatin with PEGDA for DLP-3D printable hydrogels, Eur. Polym. J. (2021) 160, https://doi.org/10.1016/j.eurpolymj.2021.110813.
[24] X. Han, et al., Advances of hydrogel-based bioprinting for cartilage tissue engineering, Front. Bioeng. Biotechnol. (2021) 9, https://doi.org/10.3389/fbioe.2021.746564.
[25] A.P. Dhand, M.D. Davidson, J.A. Burdick, Lithography-based 3D printing of hydrogels, Nat. Rev. Bioeng. 3 (2) (2025) 108–125, https://doi.org/10.1038/s44222-024-00251-9.
[26] Z. Lu, et al., Vat photopolymerization based digital light processing 3D printing hydrogels in biomedical fields: key parameters and perspective, Addit. Manuf. (2024) 94, https://doi.org/10.1016/j.addma.2024.104443.
[27] T.Y. Luo, et al., A review on the design of hydrogels with different stiffness and their effects on tissue repair, Front. Bioeng. Biotechnol. (2022) 10, https://doi.org/10.3389/fbioe.2022.817391.
[28] J. Sievers, et al., Precision hydrogels for the study of Cancer Cell Mechanobiol, Adv. Healthc. Mater. (14) (2023) 12, https://doi.org/10.1002/adhm.202202514.
[29] J. Bennett, Measuring UV curing parameters of commercial photopolymers used in additive manufacturing, Addit. Manuf. 18 (2017) 203–212, https://doi.org/10.1016/j.addma.2017.10.009.
[30] B. Grigoryan, et al., Multivascular networks and functional intravascular topologies within biocompatible hydrogels, Science 364 (6439) (2019) 458–464, https://doi.org/10.1126/science.aav9750.
[31] T. Rehbein, et al., Temperature- and degree of cure-dependent viscoelastic properties of photopolymer resins used in digital light processing, Prog. Addit. Manuf. 6 (4) (2021) 743–756, https://doi.org/10.1007/s40964-021-00194-2.
[32] M.D.A. Norman, et al., Measuring the elastic modulus of soft culture surfaces and three-dimensional hydrogels using atomic force microscopy, Nat. Protoc. (5) (2021) 16, https://doi.org/10.1038/s41596-021-00495-4.
[33] A.C. Uzcategui, et al., Microscale photopatterning of through-thickness modulus in a monolithic and functionally graded 3D-printed part, Small Sci. (3) (2021) 1, https://doi.org/10.1002/smsc.202000017.
[34] A. Vitale, J.T. Cabral, Frontal conversion and uniformity in 3D printing by photopolymerisation, Material 9 (9) (2016), https://doi.org/10.3390/ma9090760.
[35] Z.A. Zhao, et al., Indentation experiments and simulations of nonuniformly photocrosslinked polymers in 3D printed structures, Addit. Manuf. 35 (2020), https://doi.org/10.1016/j.addma.2020.101420.
[36] M.H. Khalili, et al., Mechanical behavior of 3D printed poly(ethylene glycol) diacrylate hydrogels in hydrated conditions investigated using atomic force microscopy, ACS Appl. Polym. Mater. 5 (4) (2023) 3034–3042, https://doi.org/10.1021/acsapm.3c00197.
[37] H. Gojzewski, et al., Layer-by-Layer printing of photopolymers in 3D: how weak is the interface? ACS Appl. Mater. Interfaces 12 (7) (2020) 8908–8914, https://doi.org/10.1021/acsami.9b22272.
[38] A. Saraswathibhatla, D. Indana, O. Chaudhuri, Cell-extracellular matrix mechanotransduction in 3D, Nat. Rev. Mol. Cell Biol. 24 (7) (2023) 495–516, https://doi.org/10.1038/s41580-023-00583-1.
[39] Y.Y. Li, et al., Biomaterial-based mechanical regulation facilitates scarless wound healing with functional skin appendage regeneration, Mil. Med. Res. (1) (2024) 11, https://doi.org/10.1186/s40779-024-00519-6.
[40] J.Q. Xiong, et al., Matrix stiffness affects tumor-associated macrophage functional polarization and its potential in tumor therapy, J. Transl. Med. (1) (2024) 22, https://doi.org/10.1186/s12967-023-04810-3.
[41] C. Gorsche, et al., Real time-NIR/MIR-photorheology: a versatile tool for the in situ characterization of photopolymerization reactions, Anal. Chem. 89 (9) (2017) 4958–4968, https://doi.org/10.1021/acs.analchem.7b00272.
[42] M.E. DeRosa, et al., Ultraviolet cure kinetics of a low tg polyurethane acrylate network under varying light intensity and exposure time, Prog. Org. Coat. (2021) 158, https://doi.org/10.1016/j.porgcoat.2021.106353.
[43] Q. Thijssen, et al., Radical inhibition in tomographic volumetric 3D printing for thiol-ene photoresists: from photorheology to printability, React. Funct. Polym. (2024) 205, https://doi.org/10.1016/j.reactfunctpolym.2024.106096.
[44] H.B. Zhang, et al., Controllable properties and microstructure of hydrogels based on crosslinked poly(ethylene glycol) diacrylates with different molecular weights, J. Appl. Polym. Sci. 121 (1) (2011) 531–540, https://doi.org/10.1002/app.33653.
[45] C.A. Durst, et al., Flexural characterization of cell encapsulated PEGDA hydrogels with applications for tissue engineered heart valves, Acta Biomater. 7 (6) (2011) 2467–2476, https://doi.org/10.1016/j.actbio.2011.02.018.

[46] X. Allonas, et al., Controlling photopolymerization reaction in layer-by-layer photopolymerization in 3D printing, Appl. Res. 3 (4) (2024) e202400004, https://doi.org/10.1002/appl.202400004.
[47] W.H. Carothers, Polymers and polyfunctionality, Trans. Faraday Soc. 32 (1) (1936) 39–53, https://doi.org/10.1039/tf9363200039.
[48] L.M.J. Moore, et al., Polybutadiene click chemistry: a rapid and direct method for vat photopolymerization, ACS Appl. Polym. Mater. 5 (11) (2023) 9138–9146, https://doi.org/10.1021/acsapm.3c01601.
[49] L. Schittecatte, et al., From resin formulation and process parameters to the final mechanical properties of 3D printed acrylate materials, MRS Commun. 13 (3) (2023) 357–377, https://doi.org/10.1557/s43579-023-00352-3.
[50] H.Q. Xu, et al., Effects of Irgacure 2959 and lithium phenyl-2,4,6-trimethylbenzoylphosphinate on cell viability, physical properties, and microstructure in 3D bioprinting of vascular-like constructs, Biomed. Mater. (5) (2020) 15, https://doi.org/10.1088/1748-605X/ab954e.
[51] A.K. Nguyen, et al., Toxicity and photosensitizing assessment of gelatin methacryloyl-based hydrogels photoinitiated with lithium phenyl-2,4,6-trimethylbenzoylphosphinate in human primary renal proximal tubule epithelial cells, Biointerphases 14 (2) (2019), https://doi.org/10.1116/1.5095886.